Aalto University

Author(s):   Shen, Boxuan & Linko, Veikko & Dietz, Hendrik & Toppari, J. Jussi

Title: Dielectrophoretic trapping of multilayer DNA origami nanostructures and DNA origami-induced local destruction of silicon dioxide

Dielectrophoretic trapping of multilayer DNA origami nanostructures and DNA origami-induced local destruction of silicon dioxide

Boxuan Shen[1,+], Veikko Linko[2,3,4,+], Hendrik Dietz[2] and J. Jussi Toppari[1,*]

[1] Nanoscience Center, Physics Department, University of Jyväskylä, P.O. Box 35, FI-40014 Jyväskylä, Finland

[2] Walter Schottky Institute, Physics Department, Technische Universität München, D-85748 Garching near Munich, Germany

[3] Biohybrid Materials, Department of Biotechnology and Chemical Technology, Aalto University, FI-00076 Aalto, Espoo, Finland

[4] Molecular Materials, Department of Applied Physics, Aalto University, FI-00076 Aalto, Espoo, Finland

[+] Equal contribution authors

[*]E-mail: j.jussi.toppari@jyu.fi

Abstract

DNA origami is a widely used method for fabrication of custom-shaped nanostructures. However, to utilize such structures, one needs to controllably position them on nanoscale. Here we demonstrate how different types of three-dimensional scaffolded multilayer origamis can be accurately anchored to lithographically fabricated nanoelectrodes on a silicon dioxide substrate by dielectrophoresis (DEP). Straight brick-like origami structures - constructed both in square- (SQL) and honeycomb lattices (HCL) - as well as curved 'C'-shape and angular 'L'-shape origamis were trapped with nanoscale precision and single-structure accuracy. We show that the positioning and immobilization of all these structures can be realized with or without thiol-linkers. In general, structural deformations of the origami during the DEP-trapping are highly dependent on the shape and the construction of the structure. The SQL brick turned out to be the most robust structure under the high DEP-forces, and accordingly, its single-structure trapping yield was also highest. In addition, the electrical conductivity of single immobilized plain brick-like structures was characterized. The electrical measurements revealed that the conductivity is negligible (insulating behavior). However, we observed that the trapping process of the SQL brick equipped with thiol-linkers tended to induce an etched 'nanocanyon' in the silicon dioxide substrate. The nanocanyon was formed exactly between the electrodes, i.e., at the location of the DEP-trapped origami. The results show that the demonstrated DEP trapping technique can be readily exploited in assembling and arranging complex multilayered origami geometries. In addition, DNA origamis could be utilized in DEP-assisted deformation of the substrates onto which they are attached.

1 Introduction

During the last three decades, DNA has become an extensively utilized material in nanoscale fabrication aiming towards bionanotechnological applications [1]. Today, one of the most applied techniques in structural DNA nanotechnology is a DNA origami [2], which is based on folding a long single-stranded DNA into a desired shape with the help of a set of short oligonucleotides. DNA origami enables fabrication of various two- (2D) [2] and three-dimensional (3D) [3] shapes with designed curvatures, twists and bends [4,5]. Recently, also scaffold-free origamis [6,7] and origamis based on 3D meshing have been produced [8]. Functionalization of these custom-built structures and patterning on them can be realized with nanometer precision, which opens up numerous attractive opportunities in designing tailored devices such as drug delivery vehicles [9,10], artificial ion channels [11] and molecular-level electronic circuits [12]. The rapid growth of the field - including current trends and the recent intriguing applications - has been extensively reviewed in references [13,14].

To characterize the properties of DNA nanostructures and especially to make use of them in diverse applications, these structures have to be incorporated into larger systems/networks. That requires controllable anchoring of the structures to specific areas on a chosen substrate. There exist several ways to immobilize DNA objects to the desired locations on a chip, such as chemical (thiol-based) attachment combined with standard lithographic methods [15,16], attachment to structure-specific lithographically fabricated confined spaces [17] and guiding/anchoring them to electrodes or solid-state nanopores using electric fields [18-20]. The exact positioning of DNA origamis further enables a nanoscale platform, e.g., for examining single-molecule level reactions [21] or translocations of molecules [19,20]. In addition, studying mechanical [22] and electrical [22,23] properties of single DNA origamis becomes possible when the structures are precisely integrated into the measurement setup.

In this article we present a dynamic dielectrophoresis (DEP) [24] –based trapping and immobilization method of four structurally distinct 3D multilayer DNA origami objects. The trapping and subsequent immobilization of the origami structures were achieved by applying an AC voltage to lithographically fabricated nanoelectrodes on a silicon dioxide (SiO$_2$) substrate. The presented method enables trapping with single-structure precision, thus providing a platform for various applications in nanotechnology. Although there exist reports on trapping of DNA molecules [25-31] and other DNA structures [31,32] by electric fields, so far only 2D DNA origamis have been precisely trapped by DEP [18]. Therefore, this is the first demonstration of successful DEP-based trapping and immobilization of the 3D multilayer DNA origami structures.

The origami objects used in the experiments are shown in Figure 1. We used two straight brick-like shapes stacked either in square- (SQL) [33] or honeycomb lattice (HCL) [3] of DNA helices, and two other structures having either a curved 'C'-shape or an angular 'L'-shape in honeycomb lattice (HCL). Previous work has revealed that 2D and 3D origamis can be substantially deformed under high electric fields [18,22]. For this reason, we examined the influence of the trapping force (electric field gradient) on the structural deformation of the origamis and tuned the trapping parameters accordingly. Further, we explored the effect of the origami geometry to the single-structure trapping yield and the influence of thiol-linker modifications (incorporated into the origami structures) on the immobilization characteristics.

Furthermore, the electrical conductivity of a single plain brick-like structure was characterized revealing highly resistive behavior. However, when the thiol-linkers were incorporated into the ends of the origami structure for potentially more appropriate immobilization and covalent contacts, we observed an abrupt formation of a well-defined etched area in the SiO_2 substrate strictly between the fingertip-type electrode pair. The definite mechanism of this origami-induced 'nanocanyon' formation during the DEP-trapping is not completely clear, but according to our results the thiol-modifications considerably enhance the observed phenomenon. The canyon formation was most efficient by a thiol-modified brick packed in SQL.

The reported results shine light onto the mechanical and electrical properties of multilayer origami structures under high electric fields. The proposed trapping method could readily find applications in organizing complex origami shapes into larger assemblies. Moreover, the origami-induced physical deformation of SiO_2 could be employed in DNA-based nanofabrication similarly as the previously reported chemical patterning of oxide layers by means of origami templates [34,35].
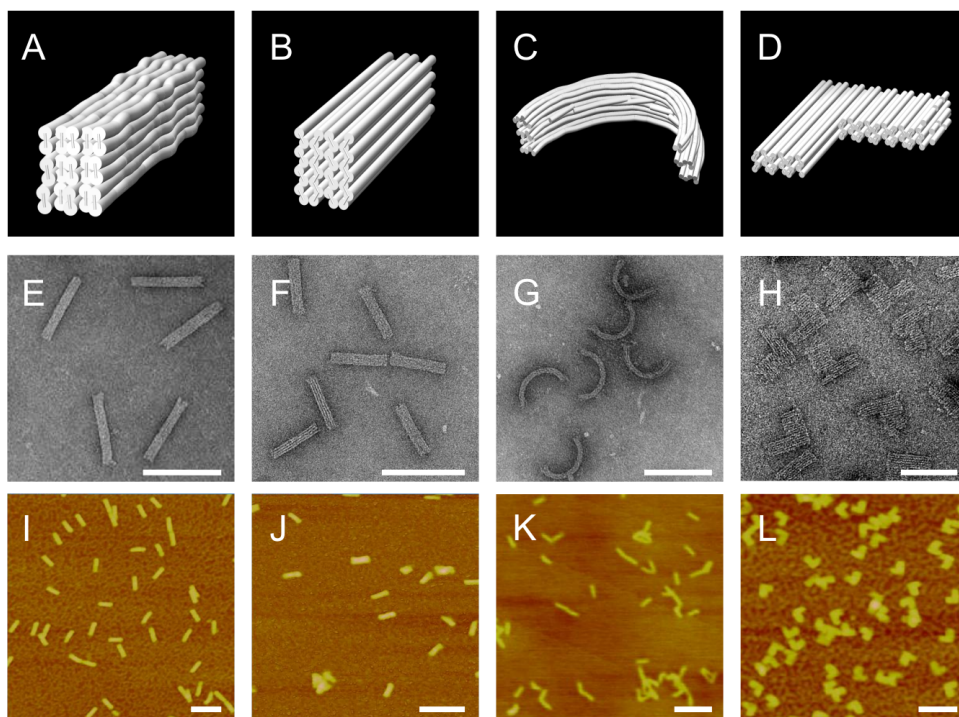
Figure 1: CanDo-simulated [36] solution shapes of the multilayer DNA origamis (A-D) used in the trapping experiments, as well as TEM (E-H) and AFM images (I-L) of the same structures: (A), (E) & (I) 30-helix bundle 'brick' in square lattice (SQL); (B), (F) & (J) 32-helix bundle 'brick' in honeycomb lattice (HCL); (C), (G) & (K) curved 'C'-shape; (D), (H) & (L) angular 'L'-shape. The 'C' and 'L' are constructed in HCL. The scale bars are 100 nm in TEM images and 200 nm in AFM images.

2 Materials and methods

2.1 DNA origami fabrication and purification

DNA origami structures were designed using caDNAno software v0.2 [37]. All the structures were designed in a honeycomb lattice (HCL) except a 30-helix brick, which was constructed in a square lattice (SQL). DNA oligonucleotide strands, i.e. so-called staples, were produced by solid-phase chemical synthesis (Eurofins MWG) with high purity salt-free purification grade (Eurofins MWG). The folding buffer of origamis contained 5 mM Tris-base, 1 mM EDTA, 20 mM $MgCl_2$, and 5 mM NaCl (pH 8). For the scaffold strand, 7249 (C-shape), 7560 (30-helix & 32-helix bricks) or 7704 (L-shape) base long M13mp18-phage-derived genomic DNA was used at 20 nM concentration. Staple strands (including optional thiol-modifications) were added with 10× excess (200 nM) to the scaffold strand. For folding the structures the temperature was ramped from 65 to 60 °C at 15 min/°C and from 59 to 40 °C at 3 h/°C [38]. Finally, the ready structures were stored at 4 °C. The quality of the folding was verified by 2 % agarose gel electrophoresis (running buffer 0.5x TBE with 11 mM $MgCl_2$) showing that all structures were folded with an acceptable yield (the quality was also verified by TEM and AFM imaging, as shown in Figure 1). The excess staple strands were removed by spin-filtering (Amicon Ultra filters with MWCO 100 kDa) and through the filtering the buffer was exchanged to a lower conductivity Hepes/NaOH-based buffer (see Section 2.3) in order to improve the DEP efficiency. When thiolated strands were incorporated into the ends of the origamis, dithiothreitol (DTT) was added to the final solution as a reducing agent in order to break disulfide bonds.

2.2 Electrode fabrication

Two different electrode geometries were used: 1) straight electrodes - used for trapping of unmodified plain structures and characterizing their electrical properties - and 2) electrodes containing titanium resistors near the gap - used for trapping of thiolated structures (see Sections 3.2 and 3.3 for their specific use). In both cases electrodes were fabricated on a slightly boron-doped (100)-silicon substrate with 200 nm thick thermally grown silicon dioxide (SiO_2) on the top. Polymethylmethacrylate (Microchem A2 PMMA) resist was spin-coated at 2000 RPM and baked for 5 minutes on a hot plate (160 ^{o}C). After patterning by an electron beam lithography system (Raith eLine), the resist was developed by immersing the sample in a mixed (1:3) solution of methyl-iso-butylketon (MIBK) and isopropyl alcohol for about 30 seconds at room temperature (22 ^{o}C). After that the sample was rinsed in isopropyl alcohol. Undeveloped residues from the mask openings were removed using a short flash of oxygen plasma in a reactive ion etcher (RIE) (Oxford Plasmalab 80 Plus). Subsequent evaporation of metal took place in an ultrahigh vacuum (UHV) chamber (pressure 10^{-8} mbar during the evaporation). After evaporation, the PMMA mask was removed by lift-off in hot acetone. Before trapping, possible PMMA residues were removed from the substrate by oxygen plasma, which also made the surface hydrophilic.

For straight electrodes the evaporation of metal was carried out at 0° angle. The thickness of the evaporated gold layer was 20 nm, under which 2-3 nm of titanium was deposited as an adhesion layer. The fabrication process was same as e.g. in Ref. [18]. The incorporation of the Ti-resistors into the electrodes was realized by utilizing an angle evaporation. Evaporation of 10 nm of titanium was done again at 0° angle. However, the subsequent gold evaporation was done at ~70° angle in the direction of

the gap, so that on the parts perpendicular to the gap, gold was not deposited on the substrate but on the walls of the resist instead. After the lift-off procedure only a thin Ti-layer having high resistance, ~70 kΩ, was left on these parts. 10 nm thick gold layer was evaporated from both directions (±70°) to ensure a correct width of the gap. An AFM image of typical electrodes with embedded Ti-resistors is shown in Figure 2A.

2.3 DEP-trapping of DNA origami

DEP experiments were performed by incubating a 5 µL droplet of spin-filtered low conductivity origami solution (buffer: 6 mM Hepes, 2 mM NaOH and 3 mM magnesium acetate, conductivity 275 µS cm^{-1}) on the surface of a chip with the nanoelectrodes for 1-5 minutes while simultaneously applying a sinusoidal AC voltage to the electrodes. When exploring the optimal trapping parameters, the DEP frequency was varied from 8 to 13 MHz, and the voltage from 0.6 to 1.5 V$_{pp}$ (peak-to-peak value). After trapping, the sample was gently washed with deionized water and dried by a flow of dry nitrogen. With careful tuning of the DEP parameters (see Section 3.1 for the detailed parameters), it is possible to trap and precisely immobilize a single origami structure between the nanoelectrodes. Schematic view of the trapping procedure is shown in Figure 2B.

2.4 TEM and AFM imaging

For the TEM imaging, the folded (either purified or unpurified) origami structures were deposited onto glow-discharged formvar-supported carbon-coated Cu400 TEM grids and negatively stained using a 2 % aqueous uranyl formate solution containing 25 mM NaOH. Imaging was carried out using a transmission electron microscope (Philips CM100) at 100 kV acceleration voltage. Images were acquired using an AMT 4x4 Megapixel CCD camera.

For the AFM imaging, the spin-filtered origami structures were deposited onto a mica surface, incubated for 2 min and dried with a nitrogen flow. All samples (including samples after the DEP trapping) were imaged using a tapping mode AFM (Veeco Dimension 3100).

2.5 Electrical measurements

DC-conductivity of single SQL and HCL bricks immobilized between the nanoelectrodes was measured at distinct relative humidity (RH) levels and compared to similar measurements made for control samples (see Section 3.2). The bias voltage was applied from a homemade low noise battery powered voltage source. While sweeping the voltage through the range of ±0.3 V, the current was measured via highly sensitive current pre-amplifier (DL-instruments 1211) capable of measuring pA currents. Finally, both the voltage and the measured current were recorded by a PC running a LabView program (National Instruments).

Moreover, the electrical properties of trapped bricks were characterized by AC impedance spectroscopy (AC-IS) [23,32] within the frequency range from 97 mHz to 100 kHz. The amplitude of the applied AC bias voltage was 50 mV. For the AC-IS measurements, two Stanford Research 830 lock-in amplifiers equipped with a general-purpose interface bus (GPIB) were connected to a computer running a specific

LabVIEW program. All the measurements were done in electromagnetically shielded room, and using the straight electrode geometry.

3 Results and discussion

3.1 DEP trapping of origamis and immobilization to gold nanoelectrodes

All the four types of 3D DNA origami structures shown in Figure 1 were successfully trapped and immobilized by DEP. Single brick-like structures, constructed either in SQL (30-helix brick) or HCL (32-helix brick) could be trapped and immobilized exactly between the opposing fingertip-type electrodes by careful tuning of the trapping parameters. After trapping, the SQL brick maintained its shape appropriately, but the bricks constructed in HCL were usually slightly deformed and flattened on a substrate, as seen in Figures 2C and 2D. Furthermore, the precise immobilization enabled us to measure the electrical conductance of single brick bridging the gap (see Section 3.2).

Moreover, we demonstrated that single 'C' and 'L'-shaped origamis (in HCL), could be equally trapped and immobilized. However, it was rather challenging to achieve high yields and clearly recognizable shapes of the structures bridging the electrodes. As one can see from the AFM images (Figure 2E and 2F), a bunch of 'C' and 'L'-structures could be gathered to the vicinity of the gap, but it is difficult to distinguish the actual shape of the object in the gap (more images of the trapped origamis can be found in Supporting Information). Plausibly, different origami shapes can have slightly distinct polarizability properties; 'L'-shape is flat, whereas the other origamis have rod-like shapes (see Figure 1). This can induce the differences on the trapping. The 'C'-shape, for one, turned out to be especially sensitive to the high electric field gradients. Deformations were clearly observed after trapping as seen in Figure 2E. This can be attributed to the structural properties of the object. The curvature was created by adding local base skips and loops into the design that further induce a global bending of the object via internal stresses [4]. As seen in Figure 1K, some structures might have straightened already when they were deposited   and immobilized onto an AFM substrate. However, TEM images (Figure 1G) show that under those particular conditions origamis can maintain their shape decently.

The optimal results in trapping of single structures or small bundles were obtained when the DEP frequency was tuned to 12.5 MHz, and voltage (peak-to-peak) to 0.8 – 1.5 V_{pp}. Trapping time was varied from 3 min to 5 min and the sample concentration was 1/50 – 1/20 of a filtered sample concentration (estimated concentration after filtration was ~10 nM). The optimal parameters for each DNA origami object are listed in the Table 1. The modest variations in the parameters are due to the slightly different geometries of the electrodes, the size and the shape of the origami (distinct polarization properties of the structures) and the concentration of origamis in the trapping solution (the exact concentration after spin-filtering is demanding to control exactly). It was observed that all types of origami structures were efficiently immobilized to the gold nanoelectrodes with or without the thiol-linkers indicating the covalent sulphur-gold bonds are not necessarily needed for the appropriate immobilization [18,23].

The trapping yields (number of samples showing positive trapping results divided by a number of total samples used) are shown in Table 1. Three out of four types of origamis have total trapping yields higher

than 50 %, which demonstrates the feasibility of the method. It should be noted, that the total trapping yield could easily reach 100 %, if the trapping voltage was raised and/or the concentration of DNA origamis in a DEP solution was increased. However, in this case the probability to trap only a single structure between the electrodes (single-structure trapping) becomes minimal. Thus, the yields shown in Table 1 are achieved with the carefully tuned parameters that maximize the chances to trap just a single object. The single-structure trapping yields were 20 % or more for both brick-like origamis. In general, it seems that multilayer 3D origamis perform reasonably well under DEP, since the single-structure trapping yields exceed 10 % yield reported for 2D origamis [18].

Table 1: Optimized DEP-parameters for 'single-structure trapping' and the trapping yields of DNA origami objects achieved by using these parameters. In total, 121 samples were used in the experiments.

|	30-helix brick (SQL)	32-helix brick (HCL)	Curved 'C'-shape (HCL)	Angular 'L'-shape (HCL)
Voltage (V_{pp})	0.9	0.9	0.8	1.5
AC-frequency (MHz)	12.5	12.5	12.5	12.5
Dilution ratio	1/50	1/50	1/20	1/50
Trapping time (min)	5	5	5	3
Total trapping yield	52 %	60 %	63 %	40 %
-Single structure	31 %	20 %	10 %	13 %
-Small bundles	21 %	40 %	53%	27 %
Empty sample	48 %	40 %	37 %	60 %
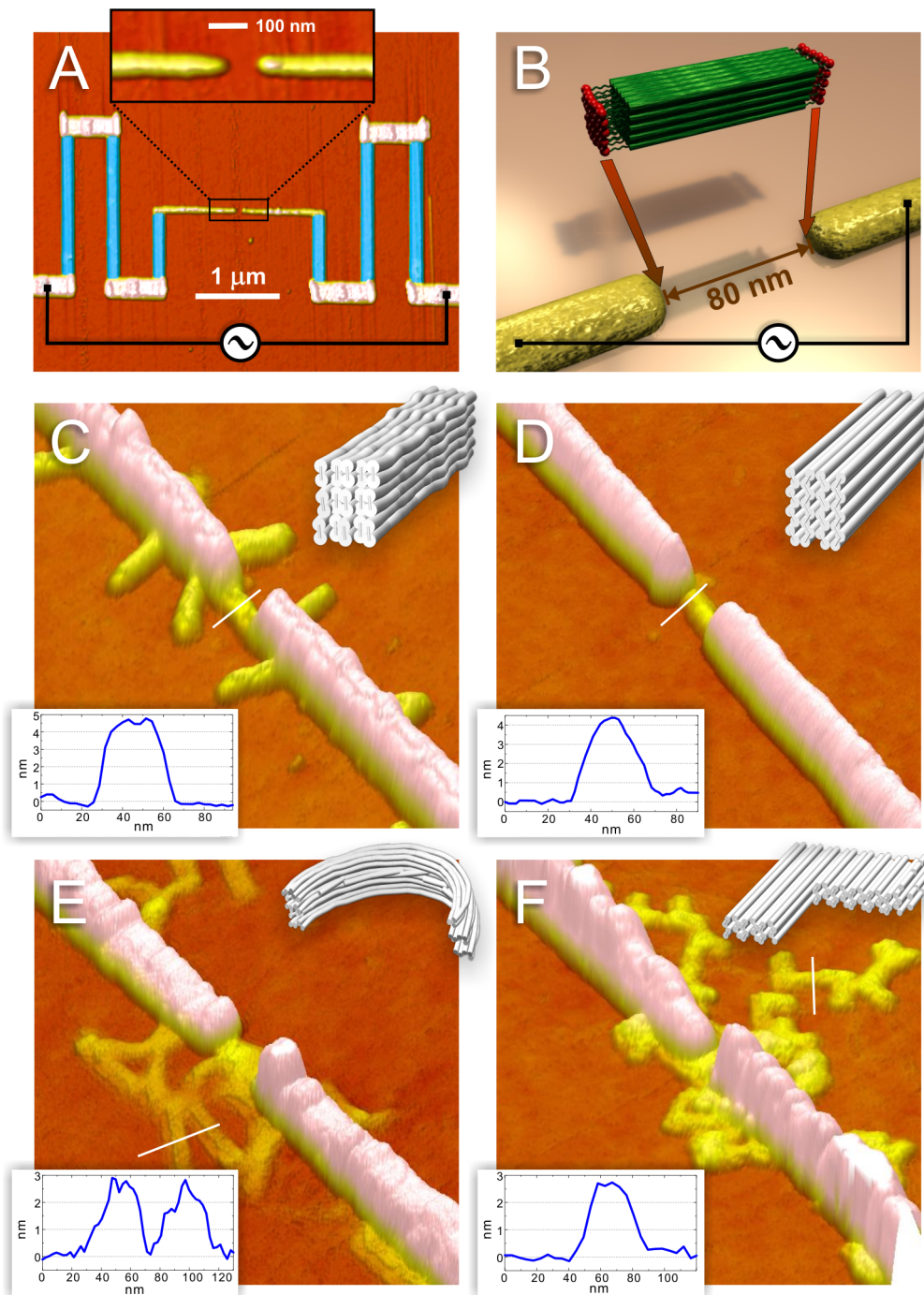
Figure 2: (A) AFM image of gold nanoelectrodes with embedded Ti-resistors (marked as blue false color). This setup was used for DEP-trapping of thiol-modified origami structures. Width of the electrodes near the gap is ~30 nm and the gap size is about 80 nm. The inset shows a zoomed-in image of the gap region. (B) Schematic view of trapping a brick-like DNA origami (with thiol-linkers) by DEP. (C) – (F) AFM images of distinct 3D multilayer origami structures trapped between the gold nanoelectrodes: (C) 30-helix brick in SQL; (D) 32-helix brick in HCL; (E) 'C'-shape in HCL; (F) 'L'-shape in HCL. The lower left insets show a cross-section along the white line on the AFM images. The upper right inset is the CanDo-simulated [36] image of the origami structure.

3.2 Electrical conductivity of single unmodified DNA origami structures

Characterization of the DC electrical resistance of a single unmodified (without thiol-linkers) brick-like origami (both 30-helix and 32-helix) immobilized exactly between the nanoelectrodes (straight electrode geometry) was carried out at room temperature both in dry conditions and at 90 % relative humidity (RH). The results were compared to similar measurements made for control samples; samples treated similarly as the origami samples except the trapping solution did not contain any origami structures (or any other DNA) (the same method was used in Refs. 23 and 32). The obtained resistance values varied from 30 GΩ to over 200 GΩ, which indicates an insulating behavior of a plain multilayer DNA origami. Examples of current-voltage (IV) curves measured from three samples and a control are shown in Figure 3A.

In addition, the electrical properties were characterized in more detail by AC-IS (see section 2.5). Measured frequency-dependent impedance for one of the trapped SQL brick is presented as a Cole-Cole plot in Figure 3B. Within the whole frequency range, both the imaginary and the real part of the impedance of 3D DNA origami were considerably higher than the values measured previously for 2D origami or (2D) TX-tile structures [23,32]. The impedance data measured from the origami samples resembled the controls. This clearly indicates an insulating behavior. AC-IS measurement were carried out at the high humidity (RH = 90 %).
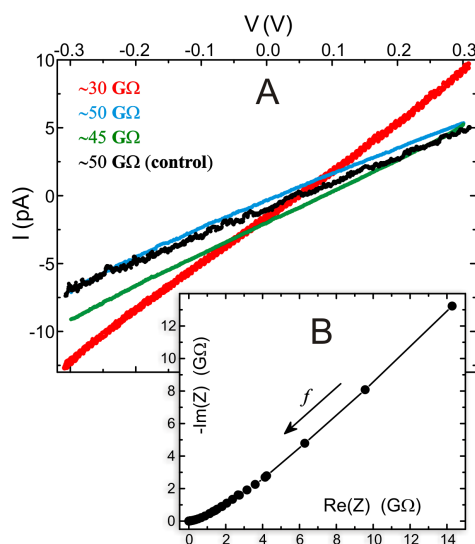
**Figure 3:** (A) IV-curves measured from trapped and immobilized single unmodified 30-helix brick origamis in SQL in high relative humidity conditions (RH ~90 %) (color data). Black data points were measured from a control sample. (B) Results of the AC-IS measurements presented as a Cole-Cole plot for one of the samples shown in (A). Arrow points the direction of increasing frequency, i.e. from 97 mHz to 100 kHz.

3.3 Nanocanyon formation by thiolated DNA origami structures

Since the observed fully insulating behavior of the plain origami structures is controversial among the results reported earlier [23,32,39,40], thiol-linkers were incorporated into the ends of the SQL brick origamis (18 thiols per each side) in order to see if a potential enhancement of the conductance would take place. Surprisingly, the trapping of the thiol-modified SQL bricks resulted in a complete destruction of the straight electrodes (electrodes utilized in electrical measurements). DEP-trapping and immobilization of thiol-modified origamis without electrode explosion was observed only in a few cases, and the electrical conductivity of these samples was subsequently characterized. Nevertheless, the resistances of such samples were in the same order of magnitude as the unmodified origamis.

Yet, it is likely that in the intact (not destructed) samples the thiol-modified SQL bricks did not form proper covalent contacts (sulphur-gold bonds) with the electrodes, which would equally explain the low electrical conductivity observed. On the other hand, in the samples containing destructed electrodes the thiol-modified origamis might have formed a covalent bond with the electrodes. The appropriate linking of the origamis to the elctrodes might have induced high local conductivity and subsequent explosion of the straight electrodes due to short-circuiting. To confirm this reasoning, titanium resistors were integrated into the electrodes (see Figure 2A and section 2.2). Consequently, additional Ti-resistors should prevent the complete destruction of the electrodes. We observed that the added resistors indeed averted the electrode destruction but instead induced a formation of a 'nanocanyon' locally in the silicon dioxide substrate. The canyon was formed exactly between the nanoelectrodes, i.e., at the position where the origami should have been trapped, as shown in Figures 4A and 4B. DEP-trapping of a thiol-modified 30-helix brick in the SQL formed well-defined nanocanyons with typical lateral dimensions similar to the width and the length of the origami. Depth of the canyon was varying from 10 to 40 nm. See Supporting information for more images of nanocanyons.
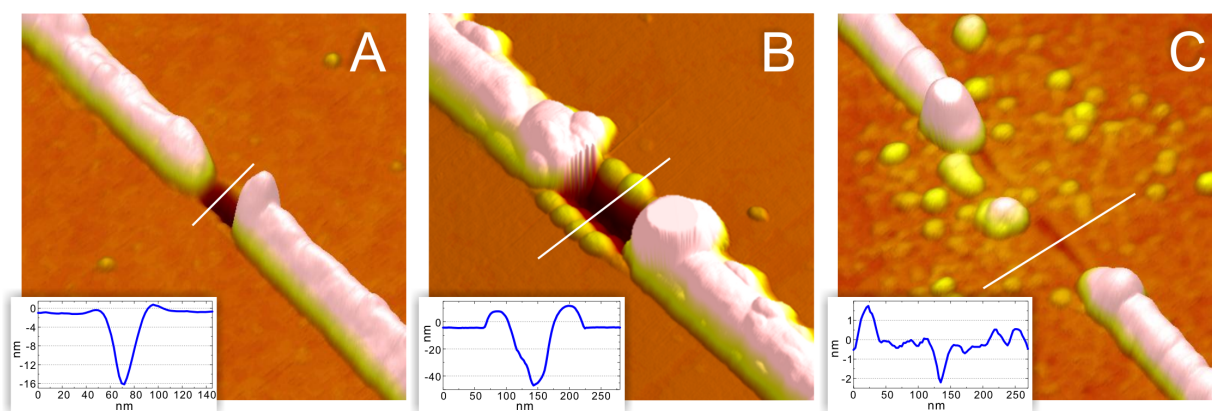
Figure 4: (A) & (B) AFM images of deep 'nanocanyons' formed after trapping of thiol-modified 30-helix bricks in SQL with 1 V_{pp}. (C) A faint 'canyon' and a minor electrode destruction created by trapping of thiolated 42 nucleotides long oligonucleotides with 5 V_{pp} as a control. In (A) and (B) the electrodes are intact, while in (C) they have been ruined within 100 - 200 nm distance from the gap.

In order to further study the nanocanyon formation, we carried out several control experiments. We incubated an electrode chip either in pure water, the trapping buffer or the buffer with high Mg++-content, while applying the DEP-voltage to the electrodes. These control experiments did not yield any canyons and even higher trapping voltages (~5 V_{pp}) were not enough to deform the electrodes or the SiO_2 substrate. We furthermore studied the canyon formation by DEP-trapping 42 nucleotides long thiolated DNA oligonucleotides [41]. By trapping the thiolated oligonucleotides the canyons were not formed until the trapping voltage was raised to as high as 5 V_{pp}. Even then, the significantly higher force (5 V_{pp} vs. 1 V_{pp}) was only enough to produce faint canyons, as seen in Figure 4C. The depth of the canyon created by extremely high DEP force and the thiolated oligonucleotides was only ~1-2 nm, which is much less than the depth of a canyon (10-40 nm) formed by the thiolated SQL brick. In addition, the shape of the canyon was not as precise, as the tips of the electrodes were destroyed within a 100-200 nm range from the gap (Figure 4C). Similar shallow and imprecise canyons were infrequently observed when unmodified origamis were trapped with remarkably high voltages. Hence, one could argue that 1) thiols enable the efficient charge transfer from the electrodes into the solution, and 2) the origami structure is needed to guide the charges to induce a local high current between the electrodes.

Taken into account that without the integrated Ti-resistors the trapping of the thiol-modified origami structures resulted in an entire destruction of the nanoelectrodes near the gap, the observations indicate that the canyon formation is related to origami-induced high currents. This could be achieved e.g. by a localized counter-ion cloud of a DNA origami (disruptive discharge) or by direct electrical conductivity via the origami at high AC-frequencies [39]. Alternatively the canyon formation could be based on the thiol-chemistry at the electrode interface(s) [42]. The yield of the canyon formation by the straight thiolated SQL brick structures was high, but in contrast, the yields were negligible when thiolated curved or angular origami shapes were trapped with the meander electrodes. The differences in canyon formation between the distinct origami shapes could be attributed to their structural properties. The helices (and therefore also the thiols) are more closely packed in the SQL brick than in other structures. Closely packed thiols and helices could plausibly cause high local currents/charge transfer at the electrode interface(s). If the DNA helices can efficiently support the charge migration, it should be noted that the bricks (both in SQL and HCL) favorably have parallel DNA helices extending from one electrode to another, whereas the helices in one arm of the L-shape are perpendicular to the electrodes. The C-shape, for one, is significantly curved. The orientation of helices could explain distinct conductivities through the gap (and thus differences in yields of canyon formation), since the conductance of helices in transverse direction (across the diameter of a helix) is negligible [43]. However, in order to thoroughly explain the observed phenomena, more comprehensive experiments are needed.

4 Concluding remarks

We have successfully demonstrated the efficient AC-DEP-based trapping and immobilization of distinct 3D multilayer DNA origami structures between gold nanoelectrodes on a SiO_2 substrate. The immobilization could be realized with or without additional thiol-linkers. The trapping yields – even single-structure trapping yields – for all four types of 3D structures used, were similar or higher than previously reported yields for 2D origamis [18]. The brick-like origami in SQL seemed to be the most robust structure for DEP trapping - it is equally the sturdiest object according to the CanDo-simulations.

DNA origamis having HCL were often deformed to some extent under high and localized electric fields (high DEP-trapping forces).

The delicate electrical measurements of unmodified immobilized bricks showed insulating behavior with the lowest resistance of a DNA origami being ~30 GΩ at RH = 90%. However, when thiol-modified SQL bricks were trapped using the electrodes containing the additional resistors, a localized and rather unexpected destruction of the SiO_2 substrate between the electrodes was observed. The trapping experiments indicate that both thiol-linkers and straight origami nanostructures are needed for formation of a well-defined nanocanyon. One reasonable explanation would be that the thiols (or other type of linkers) are required for rapid charge transfer at the electrode interface (charge transfer between the electrodes, DEP buffer and DNA), while the electrical conductivity through the gap could simultaneously be enhanced by the closely packed DNA helices or the counter-ions surrounding the DNA object. This interpretation is supported by the fact that the canyon formation yield is strongly dependent on the origami shape.

These findings are interesting in the field of molecular electronics (molecular level charge transfer and circuitry) and equally in structural DNA nanotechnology (mechanical robustness of multilayer DNA origami objects and their electrical/dielectrophoretic properties). The proposed trapping and positioning method combines the benefits of top-down and bottom-up techniques; it could readily find applications in a large-scale assembly of origami templates having high spatial patterning resolution [17]. DEP-trapping is in principle a non-destructive method for assembling unmodified 3D origamis. Although the objects might be deformed under DEP, it should be noted that they are not destructed. If one uses DNA origami merely as a simple template, DEP would be a decent method to connect origami nanostructures to the macroscopic setup. Furthermore, it could be equally possible to transfer these DEP-organized geometries to the chosen electrodeless substrates [44]. In summary, there are plenty of applications where this method could be efficiently utilized. Nevertheless, our study shows that the trapping parameters and conditions should be carefully tuned and adjusted for the optimal results. For any nanotechnological implementation where the conformation of an origami object is immensely important, e.g. if the origami template is equipped with distance-dependent functionalizations, the shape and the structural properties of the DNA origami should be deliberately chosen.

Acknowledgements

Conflict of interest statement

The authors declare no financial/commercial conflicts of interest.

5 References

[1]   N. C. Seeman, *Annu. Rev. Biochem.* **2010**, *79*, 65-87.

[2]   P. W. K. Rothemund, *Nature* **2006**, *440*, 297-302.

[3]   S. M. Douglas, H. Dietz, T. Liedl, B. Högberg, F. Graf, W. M. Shih, *Nature* **2009**, *459*, 414-418.

[4]   H. Dietz, S. M. Douglas, W. M. Shih, *Science* **2009**, *325*, 725-730.

[5]   D. Han, S. Pal, J. Nangreave, Z. Deng, Y. Liu, H. Yan, *Science* **2011**, *332*, 342-346.

[6]   B. Wei, M. Dai, P. Yin, *Nature* **2012**, *485*, 623-626.

[7]   Y. Ke, L. L. Ong, W. M. Shih, P. Yin, *Science* **2012**, *338*, 1177-1183.

[8]   D. Han, S. Pal, Y. Yang, S. Jiang, J. Nangreave, Y. Liu, H. Yan, *Science* **2013**, *339*, 1412-1415.

[9]   S. M. Douglas, I. Bachelet, G. M. Church, *Science* **2012**, *335*, 831-834.

[10]   J. Mikkilä, A.-P. Eskelinen, E. H. Niemelä, V. Linko, M. J. Frilander, P. Törmä, M. A. Kostiainen, *Nano Lett.* **2014**, *14*, 2196-2200.

[11]   M. Langecker, V. Arnaut, T. G. Martin, J. List, S. Renner, M. Mayer, H. Dietz, F. C. Simmel, *Science* **2012**, *338*, 932-936.

[12]   H. T. Maune, S. P. Han, R. D. Barish, M. Bockrath, W. A. Goddard III, P. W. K. Rothemund, E. Winfree, *Nat. Nanotechnol.* **2010***, 5*, 61-66.

[13]   A. V. Pinheiro, D. Han, W. M. Shih, H. Yan, *Nat. Nanotechnol*. **2011**, *6*, 763-772.

[14]   V. Linko, H. Dietz, *Curr. Opin. Biotechnol*. **2013**, *24*, 555-561.

[15]   A. E. Gerdon, S. S. Oh, K. Hsieh, Y. Ke, H. Yan, H. T. Soh, *Small* **2009**, *5*, 1942-1946.

[16]   B. Ding, H. Wu, W. Xu, Z. Zhao, Y. Liu, H. Yu, H. Yan, *Nano Lett*. **2010**, *10*, 5065-5069.

[17]   R. J. Kershner, L. D. Bozano, C. M. Micheel, A. M. Hung, A. R. Fornof, J. N. Cha, C. T. Rettner, M. Bersani, J. Frommer, P. W. K. Rothemund, G. M. Wallraff, *Nat. Nanotechnol*. **2009**, *4*, 557-561.

[18]   A. Kuzyk, B. Yurke, J. J. Toppari, V. Linko, P. Törmä, *Small* **2008**, *4*, 447-450.

[19]   N. A. W. Bell, C. R. Engst, M. Ablay, G. Divitini, C. Ducati, T. Liedl, U. F. Keyser, *Nano Lett.* **2012**, *12*, 512-517.

[20]   R. Wei, T. G. Martin, U. Rant, H. Dietz, *Angew. Chem. Int. Ed.* **2012**, *51*, 4864-4867.

[21]   M. B. Scheible, G. Pardatscher, A. Kuzyk, F. C. Simmel, *Nano Lett.* **2014**, *14*, 1627-1633.

[22]   C. Plesa, A. N. Ananth, V. Linko, C. Gülcher, A. J. Katan, H. Dietz, C. Dekker, *ACS Nano* **2014**, *8*, 35-43.

[23]   V. Linko, S.-T. Paasonen, A. Kuzyk, P. Törmä, J. J. Toppari, *Small* **2009**, *5*, 2382-2386.

[24]   H. A. Pohl, in *Dielectrophoresis: the Behaviour of Neutral Matter in Nonuniform Electric Field*, Cambridge University Press, Cambridge, UK. **1978**.

[25]   M. Washizu, O. Kurosawa, *IEEE Trans. Ind. Appl*. **1990**, *26*, 1165-1172.

[26]   M. P. Hughes, *Nanotechnology* **2000**, *11*, 124-132.

[27]   P. J. Burke, *Encycl. Nanosci. Nanotechnol*. **2004**, *6*, 623-641.

[28]   S. Tuukkanen, A. Kuzyk, J. J. Toppari, H. Häkkinen, V. P. Hytönen, E. Niskanen, M. Rinkiö, P. Törmä, *Nanotechnology* **2007**, *18*, 295204.

[29]   R. Hölzel, *IET Nanobiotechnol*. **2009**, *3*, 28-45.

[30]   A. Kuzyk, *Electrophoresis* **2011**, *32*, 2307-2313.

[31]   V. Linko, J. J. Toppari, *J. Self-Assembly and Molecular Electronics (SAME)* **2013**, *1*, 101-124.

[32]   V. Linko, J. Leppiniemi, S.-T. Paasonen, V. P. Hytönen, J. J. Toppari, *Nanotechnology* **2011**, *22*, 275610.

[33]   Y. Ke, S. M. Douglas, M. Liu, J. Sharma, A. Cheng, A. Leung, Y. Liu, W. M. Shih, H. Yan, *J. Am. Chem. Soc*. **2009**, *131*, 15903-15908.

[34]   S. P. Surwade, S. Zhao, H. Liu, *J. Am. Chem. Soc.* **2011**, *133*, 11868-11871.

[35]   S. P. Surwade, F. Zhou, B. Wei, W. Sun, A. Powell, C. O'Donnell, P. Yin, H. Liu, *J. Am. Chem. Soc.* **2013**, *135*, 6778-6781.

[36]   C. E. Castro, F. Kilchherr, D.-N. Kim, E. L. Shiao, T. Wauer, P. Wortmann, M. Bathe, H. Dietz, *Nat. Methods* **2011**, *8*, 221-229.

[37]   S. M. Douglas, A. H. Marblestone, S. Teerapittayanon, A. Vazquez, G. M. Church, W. M. Shih, *Nucleic Acids Res*. **2009**, *37*, 5001-5006.

[38]   J.-P. J. Sobczak, T. G. Martin, T. Gerling, H. Dietz, *Science* **2012**, *338*, 1458.

[39]   A. D. Bobadilla, E. P. Bellido, N. L. Rangel, H. Zhong, M. L. Norton, A. Sinitskii, J. M. Seminario, *J. Chem. Phys*. **2009**, *130*, 171101.

 [40]   E. P. Bellido, A. D. Bobadilla, N. L. Rangel, H. Zhong, M. L. Norton, A. Sinitskii, J. M. Seminario, *Nanotechnology* **2009**, *20*, 175102.

[41]   V. Linko, J. Leppiniemi, B. Shen, E. Niskanen, V. P. Hytönen, J. J. Toppari, *Nanoscale* **2011**, *3*, 3788-3792.

[42]   A. Bindoli, J. M. Fukuto, H. J. Forman, *Antioxid Redox Signal* **2008,** *10*, 1549-1564.

[43]   I. Katsouras, C. Piliego, P. W. M. Blom, D. M. de Leeuw, *Nanoscale* **2013**, *5*, 9882-9887.

[44]   T. K. Hakala, V. Linko, A.-P. Eskelinen, J. J. Toppari, A. Kuzyk, P. Törmä, *Small* **2009**, *5*, 2683-2686.